Eur. Phys. J. Appl. Phys. **32**, 133–141 (2005)
DOI: 10.1051/epjap:2005078

THE EUROPEAN PHYSICAL JOURNAL
APPLIED PHYSICS

New advances in ultra–stable microwave oscillators

V. Giordano[1,a], P.Y. Bourgeois[1], Y. Gruson[1], N. Boubekeur[1], R. Boudot[1], E. Rubiola[2], N. Bazin[1], and Y. Kersalé[1]

[1] Dpt LPMO Institut FEMTO–ST UMR 6174, 32 avenue de l'Observatoire, 25044 Besançon, France
[2] Université Henri Poincarré, ESSTIN and LPMIA, 2 rue Jean Lamour, 54519 Vandœuvre-lès-Nancy, France

Received: 25 April 2005 / Received in final form: 9 June 2005 / Accepted: 7 July 2005
Published online: 26 October 2005 –

Abstract. We present the new advances in ultra-stable microwave oscillators recently obtained at the department LPMO of the Institut FEMTO-ST Besançon. These microwave references are based on Sapphire Whispering Gallery Mode Resonators presenting high-Q factor. Different technologies have been developed with these resonators to fulfill the new requirements in term of phase noise or frequency stability for diverse scientific and technical applications.

PACS. 84.30.Ng Oscillators, pulse generators, and function generators – 84.40.Ik Masers; gyrotrons (cyclotron-resonance masers) – 06.30.Ft Time and frequency

1 Introduction

A growing number of scientific or technical applications requires very high frequency stability oscillators. Thus a frequency stability of the order of 1×10^{-14} for integration time between 1 and 10^4 s is now required for metrology, future space programs and some tests of fundamental physics [1–3]. Besides any reduction in oscillators phase noise will improve radar systems and phase noise measurement sensitivity.

These new requirements impose to surpass the performances of the state-of-the-art quartz crystal oscillators whose short term frequency stability is limited to around 1×10^{-13}. Such a breakthough can today be effectively achieved by the Sapphire Whispering Gallery Mode Resonator technology.

The aim of this paper is to present the new advances achieved in our laboratory, related to this technology. It summarizes about ten years of research and technical works and constitutes the continuation of a preceding paper [4]. These developments have been mainly supported by the French national space and metrology agencies (CNES and BNM).

In the first section we review the main phenomena affecting the frequency stability of an electronic oscillator. The performances of classical RF and microwave sources are then compared to the new requirements in term of frequency stability and phase noise. The principle and the main characteristics of the Whispering Gallery Mode Sapphire Resonator are recalled in Section 3. The main part of this paper (Sects. 4, 5 and 6) is devoted to present the different ultra-stable oscillators we have implemented and tested in our laboratory. Section 7 relates to a new avenue: a whispering gallery mode cryogenic MASER which presents very high potential to achieve ultra-high frequency stabilities.

[a] e-mail: giordano@femto-st.fr

2 Limitations in the oscillator frequency stability

2.1 Basic definitions

The instantaneous output voltage of a frequency generator may be written as:

$$V(t) = V_0 \sin\left(2\pi\nu_0 t + \varphi(t)\right) \tag{1}$$

where ν_0 is the nominal frequency. The quantity $\varphi(t)$ denotes the time-dependent phase variations. In presence of random perturbations the spectral purity of the oscillator is commonly represented by the one-sided spectral density of the phase fluctuations $S_\varphi(f)$.

The instantaneous frequency variation $y(t)$ is:

$$y(t) = \frac{\nu(t) - \nu_0}{\nu_0} = \frac{1}{2\pi\nu_0}\frac{d\varphi(t)}{dt}. \tag{2}$$

High resolution counters are used to measure the relative frequency fluctuations $\overline{y}$ averaged over the sampling time τ. Considering two successive countings $\overline{y}_k$ and $\overline{y}_{k+1}$ we define the two sample variance or the Allan variance by

$$\sigma_y^2(\tau) = \frac{1}{2}\left\langle \left(\overline{y}_{k+1} - \overline{y}_k\right)^2 \right\rangle \tag{3}$$

where the brackets denote an averaging over a large number of data. $\sigma_y(\tau)$ is generally adopted as a measure of the fractional frequency stability in the time domain.

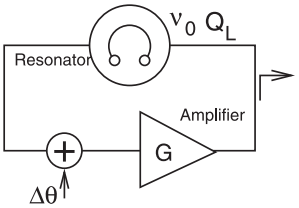

Fig. 1. Basic electronic oscillator.

A review on the tools used to characterize the frequency stability of oscillators can be found in reference [5].

2.2 Leeson formula

Basically, an electronic oscillator consists of a frequency reference, i.e. the resonator, inserted in the positive feedback loop of an electronic amplifier (see Fig. 1). The resonator is characterized by its resonance frequency ν_0 and its loaded Q-factor Q_L whereas the loop amplifier has a power gain G and a noise figure F. The signal output frequency fluctuations can arise from any phase noise source present in the loop circuit. Assume a phase variation $\Delta\theta$ arising at a given point of the circuit. As the oscillation condition imposes a constant phase along a round trip, oscillation frequency adjusts itself automatically to compensate these phase variations:

$$\frac{\Delta\nu}{\nu} = \frac{\Delta\theta}{2Q_L}. \tag{4}$$

Obviously, this phase-to-frequency conversion also takes place with random fluctuations of any part of the loop, where at higher Q-factor yield better frequency stability. This phenomena can be described by the well-known Leeson model [6] which expresses the power spectrum density (PSD) of output signal phase fluctuations $S_\varphi(f)$ as a function of the PSD of internal phase fluctuations $S_\theta(f)$:

$$S_\varphi(f) = \left(1 + \frac{\nu_0^2}{4Q_L^2}\frac{1}{f^2}\right) S_\theta(f). \tag{5}$$

An extensive discussion is available in reference [7].

2.3 Thermal noise

The fundamental limitation in the oscillator frequency stability can be derived by neglecting any internal noise source but the thermal noise. If T is the absolute temperature of the circuit and P the signal power at the amplifier input port, the PSD of the internal phase fluctuations is $S_{\theta_{th}}(f) = FkT/P$ where k_B is the Boltzmann constant. From equation (5) and for Fourier frequencies lower than the resonator bandwidth ($f < \nu_0/2Q_L$), the output signal PSD is:

$$S_{\varphi_{th}}(f) = \frac{\nu_0^2}{f^2}\frac{Fk_BT}{4PQ_l^2}. \tag{6}$$

In presence of such a white frequency noise, the oscillator frequency stability will improve as the square root of the integration time τ. Expressed as the square root of the Allan variance the frequency stability is:

$$\sigma_{y_{th}}(\tau) = \frac{1}{2}\sqrt{\frac{Fk_BT}{2PQ_L^2\tau}}. \tag{7}$$

This limitation is of the order of $2\times10^{-15}/\sqrt{\tau}$ at 1 s for a 5 MHz quartz oscillator and lower than $5\times10^{-18}/\sqrt{\tau}$ for a microwave oscillator based on a high-Q cryogenic resonator. Actual oscillators show frequency instability well above these limits and then additional noise sources have to be taken into account.

2.4 Amplifier flicker noise

In most cases, the intrinsic phase noise of the loop amplifier is the relevant noise source which limits the oscillator frequency stability at short term. For low Fourier frequencies the PSD $S_\theta(f)$ generally presents a flicker component resulting from the up-conversion of DC bias flicker [8]:

$$S_\theta(f) = (1 + f_c/f)Fk_BT/P \tag{8}$$

where f_c depends on the amplifier technology. Combining equations (5, 8), we get the oscillator phase noise for low Fourier frequencies:

$$S_\varphi(f) = \frac{\nu_0^2 f_c}{f^3}\frac{Fk_BT}{4PQ_l^2}. \tag{9}$$

$S_\varphi(f)$ appears now limited by a $1/f^3$ component leading in the time domain to a frequency instability independent of the integration time:

$$\sigma_y(\tau) = 0.59\sqrt{\frac{f_cFk_BT}{2PQ_L^2}}. \tag{10}$$

2.5 Intrinsic noise, environmental sensitivity and resonator aging

Additional frequency fluctuations of the output signal can arise from the resonance frequency fluctuations of the resonator itself. Intrinsic flicker frequency fluctuations leading to a frequency instability of the order of $0.5\text{–}1\times10^{-13}$ have been measured on high quality quartz resonators [9]. Moreover, the resonator frequency is determined by its geometry and by the wave velocity inside the resonator medium. These physical characteristics are generally affected by the environmental parameters such as the temperature, the magnetic field, the level of radiation, etc. The sensitivity to these external parameters limits the oscillator long term frequency stability. Random fluctuations in the environmental parameters lead to an oscillator stability with a $\tau^{1/2}$ slope in the Allan deviation curve.

The resonator medium properties vary with time. For example the stresses induced during the resonator mounting relax with a long time constant. As stresses induce a

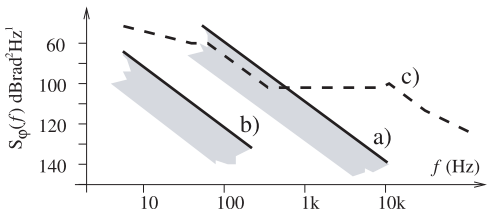

Fig. 2. Phase noise requirements (carrier frequency 10 GHz): (a) for Radar systems, (b) for metrology and fundamental physic, (c) classical 10 GHz low noise synthesized source using 5 MHz quartz reference.

change of the wave velocity in the resonator medium, the oscillator frequency drifts. These phenomena are responsible for frequency stability degradation in the long term. This aging is generally characterized in the time domain by an Allan standard deviation increasing proportionally with the integration time τ.

2.6 Frequency stability requirements

Figure 2 represents the new requirements for a 10 GHz carrier in term of phase noise for new applications in the fields of metrology, fundamental physic tests and radar systems. In the same figure the typical performance of available sources based on a quartz X-tal oscillator reference is shown. In term of frequency stability, metrology and physic experiments need secondary reference source presenting a standard deviation $\sigma_y(\tau) \leq 1 \times 10^{-14}$ over integration times ranging from 1 to typically 10 000 s.

It is obvious that these new requirements can not be fulfilled by classical quartz oscillators. This situation has motivated since about ten years a lot of researches and developments in the field of sapphire resonator based microwave oscillators which have the potential to surpass the quartz X-tal performances.

3 Whispering gallery mode resonator

The sapphire resonator consists of a cylindrical resonator machined in a low defect Al_2O_3 monocrystal. The use of particular resonance modes called Whispering Gallery (WG) modes allows to concentrate almost all the electromagnetic energy inside the sapphire cylinder. The latter has a typical diameter of 30-50 mm and a high of 10-30 mm for X-band operation. The Q-factor, essentially limited by the sapphire dielectric loss, is 200 000 at the ambient temperature, higher than 10 millions at 77 K and up to 10^9 at the liquid helium temperature. This type of resonator constitutes an excellent frequency reference that can be implemented in an oscillator loop.

In practice the sapphire cylinder is placed in the center of a metallic cavity to prevent radiation losses. Two coupling probes consisting of small magnetic loops or straight antenna protrude in the walls of the cavity and permit to excite the WG mode. In all the experiments described in the following, the sapphire resonators operate on quasi-transverse magnetic whispering gallery modes (or WGH modes). As the WG modes are high order modes, they can be perturbed by a number of low-Q spurious modes that have to be suppressed in order to get oscillation on the right resonance. We developed two different modal selection techniques enabling to operate the oscillator without the need of sharp bandpass filter in the loop [10]. The first method consists in the deposition of thin metallic lines on the flat surface of the sapphire cylinder. This technique can be applied at room temperature as well as at 77 K [11]. At lower temperature and especially around 4.2 K this method induces a strong decrease in the resonator Q-factor and then is not convenient. To address this issue we developed the opened cavity technique (see Sect. 6).

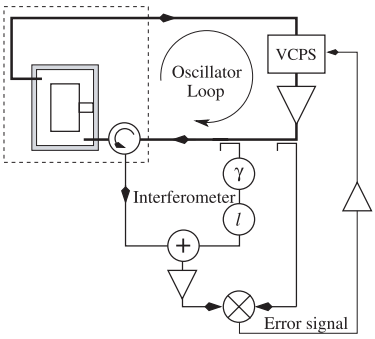

Fig. 3. WG mode sapphire resonator-oscillator with interferometric correction.

One problem with sapphire WG mode resonator is the high sensitivity to thermal fluctuations. This sensitivity arises from the strong dependence of the sapphire permittivity with temperature. Temperature stabilization and thermal compensation techniques have been then developed.

4 Room temperature oscillators

4.1 Phase noise

At ambient temperature, the sapphire resonator shows a Q-factor at least 10 times higher than classical microwave dielectric ceramic resonators. As expected from the Leeson formula (see Eq. (5)), our room temperature oscillators show a phase noise 20 dB lower than that of ceramic resonators-oscillators with similar amplifier (Fig. 4a) [4].

New generation of microwave SiGe heterostructure transistors have been tested in collaboration with the LAAS (Laboratoire d'Analyse et d'Architecture des Systèmes – Toulouse) to achieve better phase noise (see Fig. 4b) [12]. For lower noise the system has to be made more complex. A noise degeneration system can be implemented as suggested firstly by Galani [13] and improved later by Ivanov et al. [14]. In such a system the intrinsic noise of the amplifier is measured thanks to an interferometric phase noise detector that uses the sapphire resonator as phase reference (see Fig. 3). The signal reflected

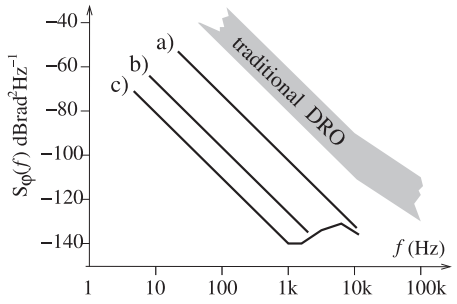

Fig. 4. Phase noise of ambient temperature 10 GHz sapphire resonator oscillators. (a) Sapphire resonator and classical AsGa microwave transistor. (b) Sapphire resonator and SiGe heterostructure microwave transistor. (c) Sapphire resonator and interferometric correction.

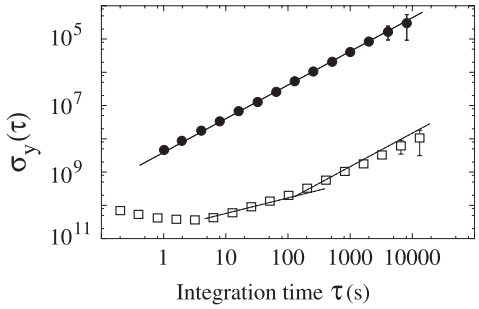

Fig. 5. Frequency stability of a room temperature WG sapphire resonator oscillator: (•) non thermally controlled, (⊡) thermally controlled.

by the resonator consists of the carrier superimposed to the phase noise modulation sidebands generated by the sustaining amplifier. A bridge comprising a variable attenuator l and a variable phase shifter γ is used to suppress the carrier. The noise sidebands are amplified and then detected with a properly pumped microwave mixer. This mixer finally delivers an error signal that is fed in a voltage controlled phase shifter (VCPS) to correct the amplifier phase noise. The interferometric technique provides in real time and with a high sensitivity a low frequency voltage proportional to the phase fluctuations induced by the amplifier [15]. Typical gain at low Fourier frequencies ($f \leq 1$ kHz) is of the order of 40 dB [16].

Figure 4 represents the phase noise for a 10 GHz carrier we obtained with the different versions of the room temperature sapphire resonator-oscillator.

4.2 Long term frequency stability

At room temperature the WG resonator suffers from a high sensitivity (–70 ppm/K) to the temperature fluctuations. It results in poor frequency stability for integration times higher than few tenth of second. A high efficiency thermal regulation has to be implemented to minimize the effect of the ambient temperature changes on the oscillator frequency. To solve this issue, we recently developed a special cavity design completed with a high-resolution thermal control [17]. The main idea is to ensure as perfect the best symmetry of the thermal paths with respect to the electromagnetic fields configuration inside the sapphire resonator. In this condition we demonstrated that the oscillator frequency stability remains limited by the intrinsic noise of the loop amplifier up to an integration time higher than 10 s (Fig. 5). At long integration time the oscillator frequency sensitivity to room temperature variation is reduced to −0.05 ppm/K.

5 Thermally compensated resonators

The oscillators described above provide high spectral purity but are not at all suited for applications requiring a high frequency stability over integration times higher than few tenth of second. Indeed the frequency stability of these oscillators is drastically limited by the resonator sensitivity to the thermal fluctuations. This sensitivity decreases slowly with temperature but remains of the order of few ppm at cryogenic temperatures. Considering the temperature can be hardly stabilized within a few 10 μK, there results in a frequency stability worst than 10^{-11} which cannot compete with the quartz oscillator.

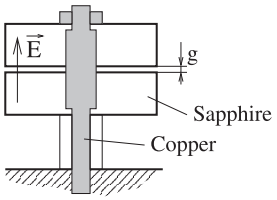

Fig. 6. Thermomechanically compensated WG mode sapphire resonator. The gap g varies with temperature.

The resonator structure has then to be modified to introduce some perturbation which will compensate the sapphire permittivity thermal sensitivity. If the compensating perturbation is well designed, the resonator shows a turnover temperature T_0 at which the thermal sensitivity nulls at the first order. The higher is the turnover temperature, the stronger is the perturbation. As the perturbation inevitably induces a degradation of the resonator Q-factor, the turnover temperature is in practice limited to $T_0 \leq 80$ K. Few compensation technics have been tested in our laboratory.

5.1 Thermomechanical compensation

The principle of the thermo-mechanical compensation (Fig. 6) has been firstly proposed by J. Dick [18].

The sapphire resonator consists of two disks separated by a small gap. The height of this gap depends on the length of a piece made in copper or silver. For a WGH mode the electric field is essentially axial. The dilatation coefficient of the copper is stronger than those of the sapphire and any increase of the resonator temperature induces an increase of the relative height of the gap. The mean value of the relative permittivity seen by the electric field then decreases which is just opposite to the natural

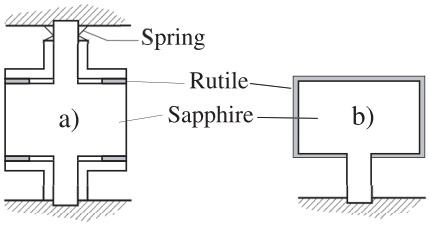

Fig. 7. Principle of dielectric compensation for cryogenic sapphire resonators. (a) Two rings of rutile are placed on the two flat surfaces of the sapphire puck and maintained by the strength of a spring. (b) A rutile thin film is directly deposited on the entire sapphire resonator surface.

sapphire relative permittivity variation. Depending on the height of the copper piece the turnover temperature can be adjusted between 40 to 90 K. We designed a compensated resonator presenting a turnover temperature of 88 K and a Q-factor of 2 millions [19].

5.2 Dielectric compensation (Fig. 7)

The sapphire shows a positive temperature coefficient of permittivity (TCP). Thermal compensation is obtained by combining sapphire with another dielectric having a negative TCP as rutile (TiO_2). Low dielectric loss rutile monocrystal can be used. The compensated resonator is a sapphire disk on which two thin rutile rings are maintained thanks to a delicat mechanical assembly. The structure we tested in our lab was designed by two other groups [20,21] and presents a turnover temperature of 53 K and a Q-factor of the order of 10^7.

We also developed another technique consisting of the deposition of a rutile film (1–2 μm thick) by using a sol–gel method on the overall surface of the sapphire disk [22,23]. The main advantage of this technique is compactness, intrinsic immunity to mechanical vibration and low cost. Nevertheless, as the deposited rutile film is not a perfect crystal, the resonator Q-factor remains limited to 2 millions. Studies on the material and on other depositions techniques are currently under development aimed to improve the crystallographic characteristic of the deposited layer.

5.3 Paramagnetic compensation

Another type of thermal compensation is obtained by doping the sapphire crystal with paramagnetic Ti^{3+} ions. The magnetic susceptibility resulting from Ti^{3+} ions depends on temperature. Its effect on the resonator frequency is opposed to those due to the sapphire permittivity sensitivity. With a 0.1% by weight Ti^{3+} ions concentration, the turnover temperature is in the range of 20–77 K, depending on the WG mode [24]. In collaboration with UWA (University of Western Australia, Perth) which provides the crystal, we tested in an oscillator loop a 25 mm diameter, 20 mm hight doped sapphire resonator excited in the $WGH_{8,0,0}$ mode at 12.7 GHz. For this mode the turnover temperature is 34.286 K and the unloaded Q-factor is 1.6×10^6.

5.4 Oscillator loop and additional control

All the above thermal compensation techniques require to cool the sapphire resonator at a cryogenic temperature. The resonator can be immersed in a liquid nitrogen or helium bath or can be mounted in a closed-cycle cryocooler. The resonator is thermally connected to the cold source and stabilized at its turnover temperature.

With a special design the sustaining amplifier can be placed in the cryogenic environment [25]. This solution yields to difficult technological issues: thermal dissipation of the microwave amplifier, final adjustment of the round-trip phase and of the overall gain in the loop. Moreover, to get high frequency stability the power injected in the resonator as well as the phase of the oscillating loop have to be controlled. These controls are difficult to implement in the cryogenic environment. Generally only the resonator is cooled while the sustaining circuit is outside the cryostat. This hybrid solution permits more flexibility in the choice of the WG mode and in the oscillator parameters, as power, gain etc. Figure 8 shows the typical circuit implemented in our oscillators.

Two semi-rigid coaxial cables link the resonator to the oscillator circuit at room temperature. The coaxial cables undergo large temperature gradients. Their electrical length fluctuates due to the cryogenic fluid evaporation or to room temperature fluctuations. There results in a large phase drift along the oscillator loop which has to be compensated. This is realized thanks to a Pound servo which ensures the oscillation frequency to be equal to the resonator frequency [26]. The loop signal is phase modulated by a voltage phase shifter inserted in the loop. The modulation frequency ν_m is higher than the resonator bandwidth. A circulator placed at the resonator input port enables to derive the signal reflected by the resonator which is sent to a tunnel diode operating as a quadratic detector. The latter delivers a voltage which is synchronously demodulated at ν_m in a locking amplifier. Let's assume that the resonator input port coupling is adjusted to the unity, i.e. $\beta_1 = 1$. The reflected signal contains the residual carrier at ν_{osc} and two sidebands at $\nu_{osc} - \nu_m$ and $\nu_{osc} + \nu_m$. When the oscillating frequency ν_{osc} is just equal to the resonator frequency ν_0, the residual carrier is absorbed by the resonator and only the two sidebands subsist. These sidebands are mixed in the diode which delivers a voltage whose a.c. component is at the frequency $2\nu_m$. The demodulated signal is then equal to zero. If $\nu_{osc} \neq \nu_0$, the diode voltage is modulated at ν_m and the demodulated signal is proportional to $\nu_{osc} - \nu_0$. The locking amplifier output signal is integrated and sent back to the bias stage of the voltage controlled phase shifter. The phase fluctuations arising in the loop are corrected in real time in the loop bandwidth. The condition $\beta_1 = 1$ is required to optimize the Pound servo operation otherwise the slope of the frequency discriminator is decreased. In practice the

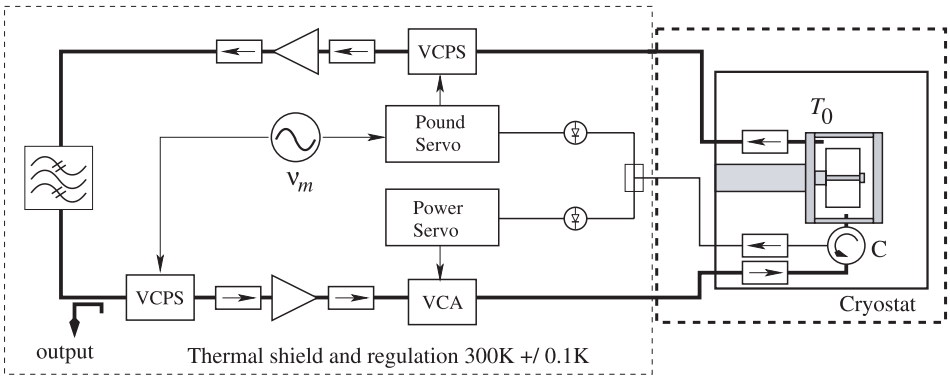

Fig. 8. Scheme of the oscillator circuit. The bold line are the oscillator loop. The thin lines refer to the electronic controls required to get a high frequency stability.

adjustment of the resonator coupling coefficients is a difficult task. Indeed as the coupling coefficients increase as the Q-factor β_1 is almost 100 times higher at cryogenic temperature than at 300 K. At room temperature, the resonator input port reflexion coefficient is hardly measurable with a network analyzer. Multiple cooldown are generally needed to get a proper value for β_1.

The sapphire resonator is also sensitive to the injected power. This sensitivity arises from two effects: the microwave power dissipation and the radiation pressure inside the resonator [27]. In our experiments we stabilized the power injected in the resonator by a classical power control using a quadratic detector as the sensor and a voltage controlled attenuator (VCA) in the loop.

Finally all the room temperature electronics are stabilized at 300 ± 0.1 K.

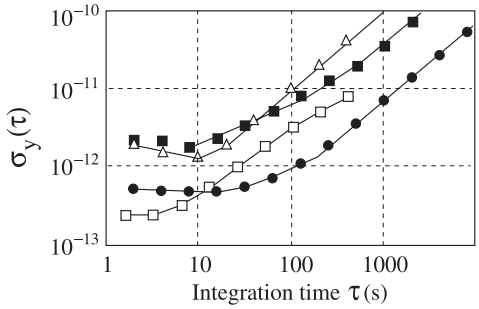

Fig. 9. Frequency stability obtained with the compensated resonators. (△) Thermomechanical compensated resonator $T_0 = 87$ K. Those of (■) Dielectric compensation with sol-gel deposited thin film of rutile $T_0 = 47$ K. (□) Dielectric compensation with mechanical assembly of monocrystal rutile rings on sapphire. (●) Ti^{3+} doped sapphire resonator.

5.5 Performances

The different compensated sapphire resonators described above have been tested alone and in actual oscillators. The performances are given in Figure 9.

These oscillators provide an improvement as compared to the non-compensated oscillators. Nevertheless, for integration time higher than few seconds, frequency drift phenomena occur, limiting the interest for these structures. The frequency drift causes have still not been clearly identified. Few phenomena can induce such long term variations, as stress or thermal gradient relaxation. Although the performances are still not sufficient, these structures are alternative solutions for the next-generation of low noise oscillators.

6 Low temperature resonator oscillator

6.1 Natural thermal compensation

In order to obtain ultra-high frequency stability, the sapphire resonator must be cooled near the liquid helium temperature, where the Q-factor of the WG modes can reach 10^9. Moreover the resonator shows a turnover temperature near 6 K. Fortunately even high quality crystals contain a small concentration ($\lesssim$1 ppm in weight) of paramagnetic impurities as Mo^{3+} ions as the consequence of the growth process. There results a natural thermal compensation at random turning point between 4 K and 10 K, depending on the actual impurities and on the mode [28]. Figure 10 shows the frequency variation of the $WGH_{16,0,0}$ resonance of a 50 × 20 mm HEMEX sapphire resonator between 4 and 10 K. The thermal sensitivity is zero at about 6 K.

6.2 Opened cavity concept

It is a common practice to enclose the sapphire in a Nb or Cu cylindrical cavity. This cavity prevents radiation losses and improve thermal stability. The main drawback of this configuration is the presence of a number of low-Q empty cavity modes perturbed by the sapphire resonator. These spurious modes induce Q-factor degradation and enhance of the thermal sensitivity [29]. To suppress these spurious modes we have used an opened cavity structure [30]. Only the metal caps remain while the cylinder is replaced with

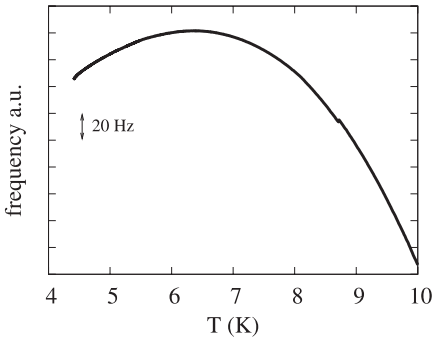

Fig. 10. $WGH_{16,0,0}$ resonant frequency as a function of temperature. The turning point occurs at 11.565051341 GHz.

Fig. 11. Picture of the opened cavity WG resonator.

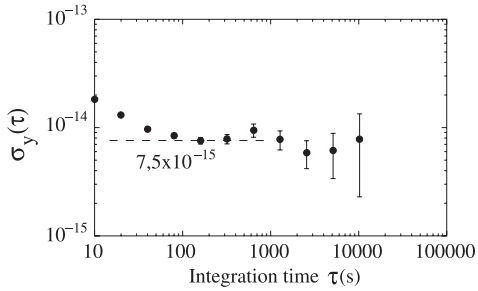

Fig. 12. Frequency stability of the cryogenic resonator-oscillator operating at 10.959 GHz.

microwave absorber (Fig. 11). This assembly is inserted in a vacuum chamber whose internal walls are covered with microwave absorber.

In this configuration the spurious resonances are no longer confined, for they are completely eliminated from the spectrum. Conversely, the high order whispering gallery modes are almost unaffected by the absorber. The measured Q-factor of these modes is still higher than 2×10^8 which is sufficient for a frequency stability of 1×10^{-14}. Figure 12 shows the frequency stability obtained with the resonator operating on the $WGH_{15,0,0}$ mode at 10.959 GHz with a Q-factor of 4.3×10^8. This measurement has been made by comparing the cryogenic oscillator frequency with a microwave synthesizer (Agilent 8254A) driven by a hydrogen maser.

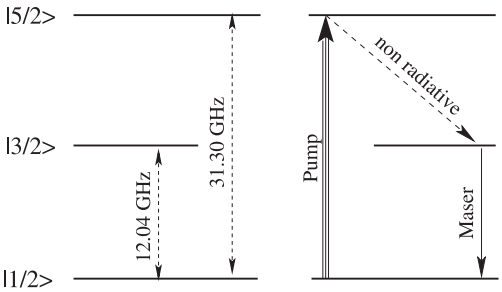

Fig. 13. Energy levels of Fe^{3+} ion in sapphire at zero dc magnetic field.

At short term, the measured stability is limited by the noise of the reference. The cryogenic oscillator instability shows up at $\tau > 100$ s. The flicker floor is of the order of 7×10^{-15}. Interestingly, no drift is observed (up to 2×10^{-14}/day) [31], while similar oscillators implemented by other groups are affected by frequency drift of the order of 1×10^{-13}/day. The cause of this fortunate outcome is still not known. Nevertheless, we believe that it results from the opened cavity. In fact, all other oscillators are based on a sapphire resonator in a closed metallic cavity. The useful mode is in this case embedded by number of spurious modes. The latter can increase the reference mode sensitivity to mechanical creeps or to thermal drift. Forthcoming experiments should permit to understand these phenomena.

7 Zero–field Fe^{3+} Maser

In the ultra-stable oscillator described above, the resonator and the sustaining amplifier are spatially separated and the oscillator requires appropriate microwave coupling and a frequency control loop. The overall system is therefore complex and need difficult adjustments. In this classical configuration the cryogenic resonator is simply a linear two-port system that provides a sharp resonance.

We have demonstrated that the sapphire resonator can be used in a different way [32]. Among the different paramagnetic impurities that can be found in high purity sapphire crystal there is the Fe^{3+} ion. The Fe^{3+} energy levels at zero dc magnetic field are shown in Figure 13. Near the liquid helium temperature, there are significant differences in the populations of these levels. Transitions between any of these levels are allowed and their linewidths are of a few tens of MHz. A 31.3 GHz pump signal causes a net transfer of Fe^{3+} ions from the $|1/2\rangle$ level to the $|5/2\rangle$ level. In turn non-radiative transitions $|5/2\rangle \mapsto |3/2\rangle$ create a negative population difference between the two lower states, making possible the amplification of a 12.04 GHz signal.

Our whispering-gallery-mode maser is represented in Figure 14. It is based on sapphire resonator whose $WGH_{17,0,0}$ mode frequency coincides with the $|1/2\rangle \mapsto |3/2\rangle$ frequency, i.e. 12.04 GHz. This resonator has a number of resonances near the pump frequency. After some attempts, we observed that a 2 dBm pump signal

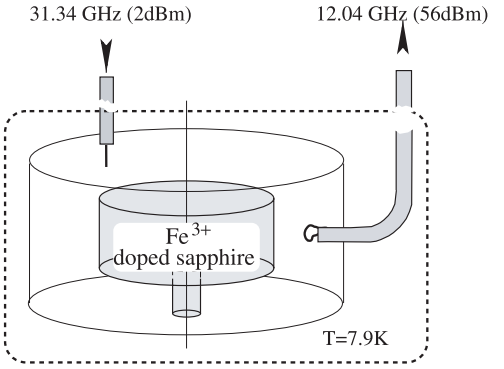

Fig. 14. Principle of the whispering gallery mode maser oscillator.

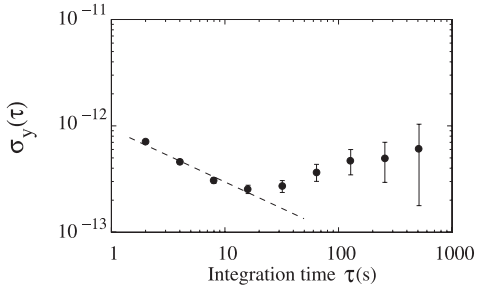

Fig. 15. Preliminary result on frequency stability of the whispering gallery mode maser. The dashed line is the noise floor of the measurement system.

at 31.34 GHz is sufficient to obtain a –56 dBm maser signal, available outside of the cryostat. The output Maser signal was directly amplified by 70 dB and mixed with the signal of a microwave synthesizer (Wiltron 69137A) driven by a hydrogen Maser. The 200 kHz beatnote is sent to a high resolution frequency counter (HP 53132A). We slowly increased the resonator temperature and recorded the beat-note frequency. We determined experimentally that the maser frequency has a turn-over point at 7.9 K. Finally we stabilized the resonator temperature at the turning point and we measured the Allan deviation σ_y of the fractional frequency (Fig. 15).

At short integration times, $\tau < 100$ s, the WG maser exhibits a frequency stability better than 4×10^{-13}. The cause of the long term degradation has still not been determined. Although the system is not optimized, this preliminary result is encouraging. For instance, the two lines linking the cryogenic resonator to the outside do not include isolators. Fluctuations in the standing wave pattern could thus induce significant drift on the maser frequency. We have to evaluate the resonator sensitivity to experimental parameters as the pump power and frequency, the resonator coupling, the reflexion coefficient of feedthrough and cables, magnetic field, etc.

The WG maser shows several advantages versus the classical oscillator: (i) there are fewer critical components, (ii) it is simpler and more compact, (iii) the number and the complexity of auxiliary controls is reduced, and (iv) the resonator coupling is far less critical.

8 Conclusion

The technology of the Sapphire Whispering Gallery Mode Resonator permits to surpass the frequency stability of traditional ultra-stable oscillators, and then can be exploited in number of applications requiring a high frequency stability. The main difficulties, i.e. thermal sensitivity and spurious modes, associated with such a type of frequency reference have been solved by means of original techniques. It has also been demonstrated that at liquid helium temperature the sapphire-resonator-oscillator shows a stability of 7.5×10^{-15} at short term and better than 5×10^{-14} over one day. Finally, we have demonstrated the maser operation of a Fe^{3+} doped sapphire. Engineering work is still needed in order to make a useful frequency standard out of our maser.

References

1. A.G. Mann, G. Santarelli, S. Chang, A.N. Luiten, P. Laurent, C. Salomon, D.G. Blair, A. Clairon, in *Proc. IEEE International Frequency Control Symposium, Pasadena, CA., 1998*, pp. 13–17
2. P. Wolf, S. Bize, A. Clairon, A.N. Luiten, G. Santarelli, M.E. Tobar, Phys. Rev. Lett. **90**, 060402 (2003)
3. V. Candelier, P. Canzian, J. Lamboley, M. Brunet, G. Santarelli, in *Proc. IEEE International Frequency Control Symposium, Tampa, FL, USA, 2003*, pp. 575–582
4. V. Giordano, Y. Kersalé, O. Di Monaco, M. Chaubet, Eur. Phys. J. Appl. Phys. **8**, 269 (1999)
5. J. Rutman, Proc. IEEE **66**, 1048 (1978)
6. D.B. Leeson, Proc. IEEE **54**, 329 (1966)
7. E. Rubiola, `arXiv:physics/0502143v1` (2005)
8. D. Halford, A.E. Wainwright, J.A. Barnes, in *Proc. of the Frequency Control Symposium, Fort Monmouth, N.Y., USA, 1968*, pp. 340–341
9. E. Rubiola, J. Groslambert, M. Brunet, V. Giordano, IEEE T. Ultrason. Ferr. **47**, 361 (2000)
10. O. Di Monaco, W. Daniau, I. Lajoie, Y. Gruson, M. Chaubet, V. Giordano, Electron. Lett. **32**, 669 (1996)
11. O. Di Monaco, Y. Kersalé, V. Giordano, IEEE Microw. Guided W. **10**, 368 (2000)
12. G. Cibiel, M. Régis, O. Llopis, A. Rennane, L. Bary, R. Plana, Y. Kersalé, V. Giordano, IEEE T. Ultrason. Ferr. **51**, 1 (2004)
13. Z. Galani, M. Bianchini, IEEE T. Microw. Theory **32**, 1556 (1984)
14. E.N. Ivanov, M.E. Tobar, R.A. Woode, IEEE T. Ultrason. Ferr. **45**, 1526 (1998)
15. E. Rubiola, V. Giordano, Rev. Sci. Instrum. **71**, 3085 (2000)
16. Y. Gruson, Y. Kersalé, E. Rubiola, C. Rocher, M. Chaubet, V. Giordano, in *Actes des 13es Journées Nationales Microondes (JNM 2003), Lille, 2003*, pp. 4C2–2
17. R. Boudot, C. Rocher, N. Bazin, S. Galliou, V. Giordano, O. Llopis, in *Proc. 19th European Frequency and Time Forum, Besançon, France, 2005*, to be published

18. G. Dick, D. Santiago, R. Wang, IEEE T. Ultrason. Ferr. **42**, 812 (1995)
19. Y. Kersalé, F. Ladret-Vieudrin, M. Chaubet, V. Giordano, IEEE T. Ultrason. Ferr. **47**, 427 (2000)
20. M.E. Tobar, J.G. Hartnett, E.N. Ivanov, D. Cros, P. Blondy, P. Guillon, IEEE T. Microw. Theory **48**, 1265 (2000)
21. J.G. Hartnett, P.Y. Bourgeois, J.D. Anstie, M.E. Tobar, N. Bazin, E.N. Ivanov, D. Cros, V. Giordano, Y. Kersalé, Electron. Lett. **40**, 1 (2004)
22. Y. Kersalé, O. Vallet, S. Vives, C. Meunier, V. Giordano, Electron. Lett. **37**, 23 (2001)
23. Y. Kersalé, N. Boubekeur, P. Bourgeois, N. Bazin, S. Vives, C. Meunier, V. Giordano, in *Proc. of the 2003 IEEE International Frequency Control Symposium, Tampa, FL, USA, 2003*
24. J.G. Hartnett, M. Tobar, A. Mann, J. Krupka, E. Ivanov, Electron. Lett. **34**, 195 (1998)
25. S. Vitusevich, K. Schieber, I. Ghosh, N. Klein, M. Spinnler, IEEE T. Microw. Theory **51**, 163 (2003)
26. A. Luiten, A.G. Mann, A. Giles, D. Blair, IEEE T. Instrum. Meas. **42**, 439 (1993)
27. S. Chang, A.G. Mann, A.N. Luiten, D.G. Blair, Phys. Rev. Lett. **79**, 2141 (1997)
28. A.N. Luiten, A. Mann, D. Blair, J. Phys. D Appl. Phys. **29**, 2082 (1996)
29. M. Tobar, J. Phys. D Appl. Phys. **26**, 2022 (1993)
30. P.Y. Bourgeois, Y. Kersalé, N. Bazin, M. Chaubet, V. Giordano, IEEE T. Ultrason. Ferr. **51**, 10 (2004)
31. P.Y. Bourgeois, F. Ladret-Vieudrin, Y. Kersalé, N. Bazin, M. Chaubet, V. Giordano, Electron. Lett. **40**, 10 (2004)
32. P. Bourgeois, M. Oxborrow, N. Bazin, Y. Kersalé, V. Giordano, in *Proc. 19th European Frequency and Time Forum, Besançon, France, 2005*, to be published